

## Optimization of transducer arrays parameters for efficient excitation of Lamb waves

L. Mažeika, R. Kažys, A. Maciulevičius

Ultrasound institute of Kaunas University of Technology,

### Abstract:

The guided waves are used for inspection of large industrial constructions. The Lamb waves are a sort of the guided waves propagating in planar structures. They can be used for inspection of such objects like metal plates and sheet piles. The regularities of the excitation of Lamb waves by single longitudinal and shear type transducers has been determined using numerical modelling. The directivity patterns of the transducers arrays having different configurations have been investigated using the results of the numerical modelling. It was found out that the main problem is not the generation of guided waves, but generation of the desired mode of a guided wave. In the case of generation of various modes under the different angles to the main wavefront direction, it is complicate to interpret the results because the waveforms of the received signal become very complicated. The obtained results revealed several configurations of the transducer arrays which enable generation only the desired mode of the Lamb wave with a relatively low level of the parasitic, e.g., undesired waves. It was also demonstrated and explained the difference between application of the longitudinal and the shear type of the transducers in ultrasonic arrays. It was pointed out the advantage of the delay time technique of excitation of transducer arrays comparing to the simultaneous excitation of all elements of the array.

**Key words:** transducer arrays, Lamb waves, directivity pattern, modelling.

### Introduction

The guided waves are used or can be used for inspection of large, elongated industrial objects such like pipes, rails, cable ropes and etc [1-4]. The Lamb waves are a sort of the guided waves which propagate in planar components of the objects. In general, propagating guided waves contain all three components of particle velocity. The different combinations of the amplitudes and phases lead to the existence of many modes. So, selective generation of the desired guided waves mode can be implemented by excitation of the specific components of the displacements (or particle velocities), matching them to the spatial and temporal properties of the desired wave. This can be implemented only exploiting *a priori* knowledge about properties of propagating guided waves and the characteristics of the used transducer. The most promising technique for generation of the selected modes is application of transducer arrays, because most of the long range ultrasonic inspection objects are plate - like structures, such as plates, sheet piles, pipes. So, the investigation presented below is devoted to determination of the regularities of the guided wave generation in plates using transducers arrays.

The main problem is optimization of the transducer array used for generation of a desired mode of guided waves. The optimization means that should be developed such a transducer array which most efficiently generates desired waves along the object and at the same time it creates a low level parasitic side lobes. The investigations were carried out in the following steps:

- The investigation of the regularities of the excitation of the Lamb waves using the single longitudinal waves and shear waves transducers;
- The analysis of the directivity patterns of the transducer arrays having different configurations and based on the different types of transducers (longitudinal and shear);

- Comparison of the different techniques of the transducer array excitation: simultaneous and using the time delay.

### The point spread function of the point source of longitudinal and shear waves

In the most cases of applications of the long range ultrasonic the dimensions of the transducers are smaller comparing to the wavelength of the excited guided waves. So, it can be assumed that the transducers are point like sources of ultrasonic waves having a wide or even a circular directivity pattern. The objective of this step was to investigate the directivity patterns of the longitudinal and the shear type point sources using the 3D finite element modelling and to estimate how efficiently the  $A_0$  and the  $S_0$  modes of Lamb wave are generated using the different types of transducers.

The investigation has been carried out using finite element model of the aluminium plate (Fig.1). The aluminium parameters are presented in the Table 1. The dimensions of the plate are 0.5x0.5m and the thickness 10mm.

Table 1. The parameters of the aluminium used in the modelling

Parameter	Value
Density, $\rho_{Al}$	2700 kg/m <sup>3</sup>
Young modulus, $E_{Al}$	70 GPa
Poisson's ration, $\nu$	0.33

For the excitation the 2 periods burst having the Gaussian envelope and the frequency 70 kHz was used. The waveform of the excitation signal is presented in Fig.2. Such a narrowband signal was selected with the purpose to have a better selectivity of the different wave modes propagating with different velocities. Two types of excitation have been analysed: the normal to the surface of

the plate (longitudinal) (Fig.1a) and the tangential (shear) (Fig.1b). The excitation force was added in the middle of the aluminium plate.

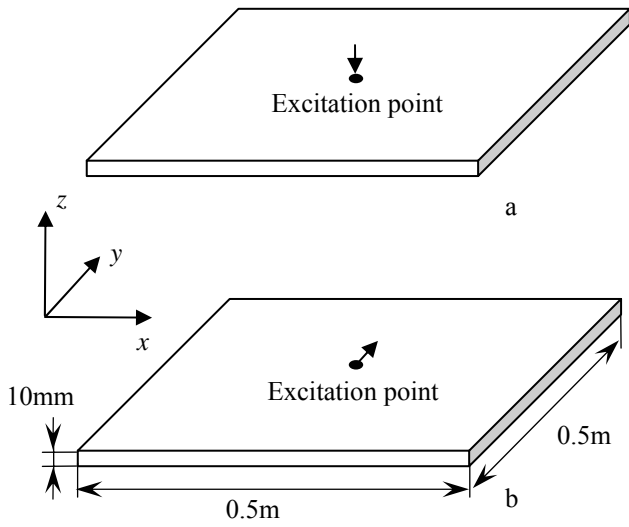


Fig.1. Investigated aluminium plates: a - the normal excitation force; b - the shear excitation force

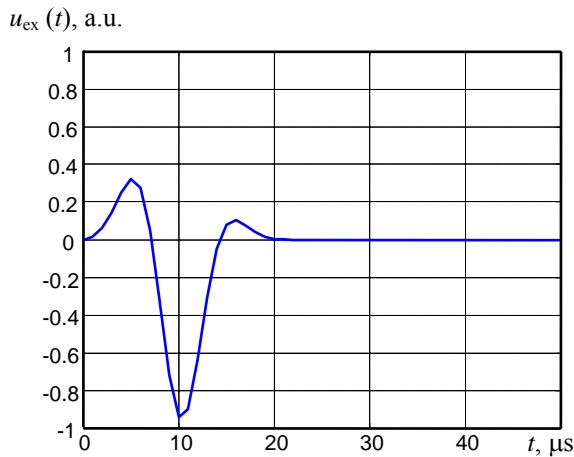


Fig.2. The waveform of the excitation signal

In the case of the normal excitation the task in principle is axi-symmetric and as a consequence the directivity patterns of both  $A_0$  and  $S_0$  modes are uniform in all directions (circular). This is demonstrated by the distribution modulus of the particle velocity  $v = \sqrt{v_x^2 + v_y^2 + v_z^2}$  at the time instant  $75\mu s$  after excitation, presented in Fig.3. So, it can be assumed that the point source of longitudinal waves generates the Lamb waves having close to the circle directivity pattern.

More complicated is application of the shear type transducers, even if to assume that they are very small comparing to the wavelength. In the case of the tangential excitation the acoustic field have a non-uniform distribution. The distribution of the normal component of a particle velocity (Fig.4) demonstrates that the  $A_0$  mode of Lamb waves propagating in the opposite direction have an opposite phase with respect to the phase of the wave

propagating to the right in Fig.4.. The distribution of the tangential component of a particle velocity  $v_\tau = \sqrt{v_x^2 + v_y^2}$  at the time instant  $50\mu s$  after excitation presented in Fig.5 demonstrates the similar features of the  $S_0$  mode Lamb wave also.

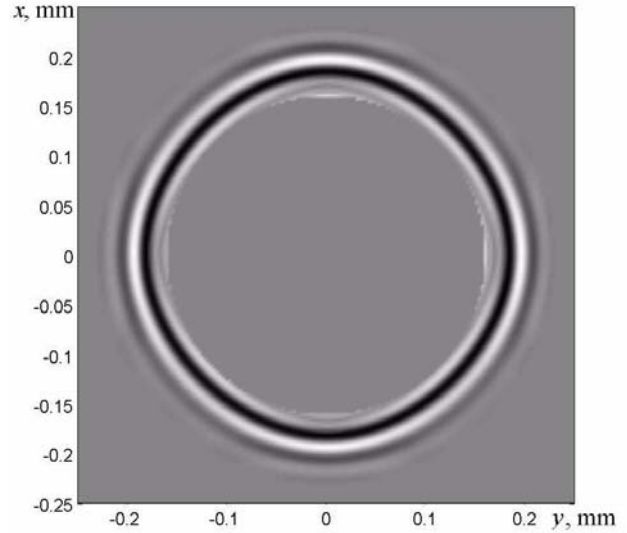


Fig.3. The distribution of the modulus of a particle velocity of the  $A_0$  mode wave at the time instant  $75\mu s$  after the excitation using the longitudinal waves point like transducer.

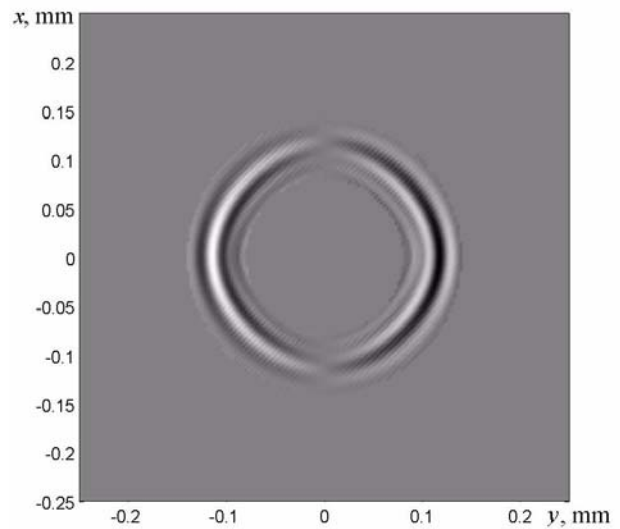


Fig.4. The distribution of the normal particle velocity  $v_{z,t=50}(x,y)$  of the  $A_0$  mode wave at the time instant  $50\mu s$  after the excitation using the shear wave point like transducer.

The directivity patterns of the tangential point source for the  $A_0$  and the  $S_0$  modes of Lamb waves were calculated using the particle velocity distribution at the time instant  $50\mu s$  according the following expressions:

$$d_{A_0}(\alpha) = \max_{R_{1,A_0} < R < R_{2,A_0}} |v_{z,t=50}(x,y)|, \quad (1)$$

$$d_{S_0}(\alpha) = \max_{R_{1,S_0} < R < R_{2,S_0}} |v_{xy,t=50}(x,y)|, \quad (2)$$

where  $d_{A_0}(\alpha)$ ,  $d_{S_0}(\alpha)$  are the directivity patterns of the  $A_0$  and  $S_0$  modes,

$v_{xy,t=50}(x, y) = v_{x,t=50}(x, y) \cdot \cos(\alpha) + v_{y,t=50}(x, y) \cdot \sin(\alpha)$ ,  
 $v_{x,t=50}(x, y)$ ,  $v_{y,t=50}(x, y)$ ,  $v_{z,t=50}(x, y)$  are  $x$ ,  $y$  and  $z$   
 components of the particle velocity at the time instant  
 $50\mu\text{s}$ ,  $\alpha = \arctan(x/y)$ ,  $R_{1,A0}$ ,  $R_{1,S0}$ ,  $R_{2,A0}$ ,  $R_{2,S0}$  are the  
 ranges of the  $A_0$  and the  $S_0$  mode waves along the radius  
 measured from the origin (zero) point.

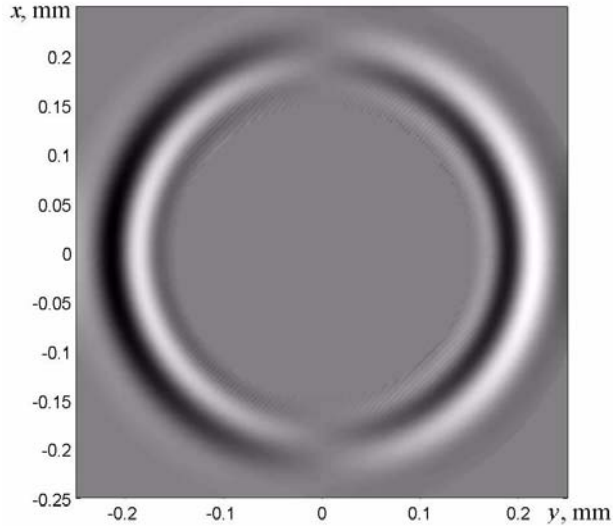


Fig.5. The distribution of the tangential particle velocity  $v_{xy,t=50}(x, y)$  of the  $S_0$  mode at the time instant  $50\mu\text{s}$  after the excitation using the shear waves point like transducer

The obtained directivity patterns are presented in Fig.6 and 7. As can be seen both of them have two lobes in front and back directions having opposite phases. There is a very weak generation in lateral direction.

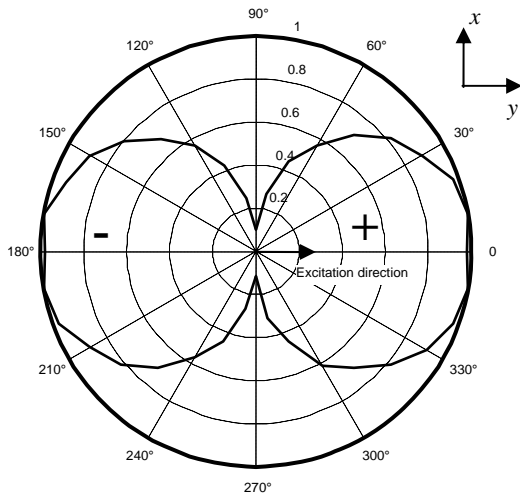


Fig.6. The directivity pattern  $d_{A0}(a)$  of the  $A_0$  mode wave in the case of the tangential excitation obtained from the results of the finite element modelling. The excitation force direction is denoted by the arrow.

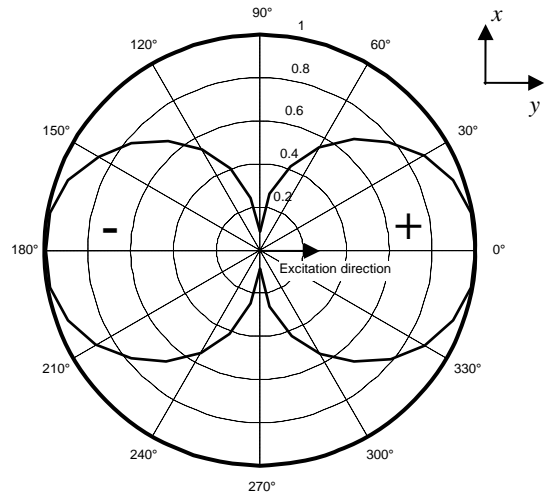


Fig.7. The directivity pattern  $d_{S0}(a)$  of  $S_0$  mode wave in the case of the tangential excitation obtained from the results of the finite element modelling. The excitation force direction is denoted by the arrow.

### Analysis of the directivity patterns of the transducer arrays having different configuration

In general for calculation of a directivity pattern of the guided waves it is necessary to use the model that enables to take into account dispersion phenomenon. On the other hand in most long range applications generation of the guided waves is performed at the frequencies which are outside strong dispersion ranges. Taking all this into account the simplified directivity pattern calculation technique has been developed.

The calculation of the directivity pattern of a transducer array is based on: the known position of the transducer array element  $x_{te,k}$ ,  $y_{te,k}$ ,  $k = 1 \div N_{te}$ ,  $N_{te}$  is the number of the transducer elements; the known group  $c_g$  and phase  $c_{ph}$  velocities of the guided waves under analysis. The directivity pattern the transducer array was calculated according to

$$d_{ta}(\alpha) = \max_t [u_{\Sigma}(\alpha, t)] - \min_t [u_{\Sigma}(\alpha, t)], \quad (3)$$

where

$$u_{\Sigma}(\alpha, t) = \sum_{k=1}^{N_{te}} u_k(\alpha, t), \quad (4)$$

$u_k(\alpha, t)$  is the signal generate by the  $k^{\text{th}}$  element of transducer array under the angle  $\alpha$ .

For calculation of the signal generated at some angle the distance  $d$  between the centre of the transducer array  $O_{TA}(x_{TA}, y_{TA})$  and the observation point  $O_P(x_P, y_P)$  was selected relatively big to be in a far field zone of the transducer array. In the case under analysis it was 5 m. The position of the observation point is calculated according to

$$\begin{aligned} x_P &= d \cdot \sin(\alpha) + x_{TA} \\ y_P &= d \cdot \cos(\alpha) + y_{TA} \end{aligned} \quad (5)$$

The signals at the observation point given by

$$u_k(\alpha, t) = e^{-a^2(n_p, t-t_p)} \cdot \sin(2\pi ft - \Delta t_{ph}), \quad (6)$$

where  $a(n_p, t-t_p)$  is the normalization coefficient dependent on the number of the periods  $n_p$  in the signal and the wave energy propagation time  $t_p$ ,

$$t_p = \frac{\sqrt{(x_P - x_k)^2 + (x_P - x_k)^2}}{c_g},$$

$$t_{ph} = \frac{\sqrt{(x_P - x_k)^2 + (x_P - x_k)^2}}{c_{ph}},$$

$$\Delta t_{ph} = (t_{ph} - t_g) \cdot f \cdot 2 \cdot \pi,$$

$f$  is the central frequency of the signal.

Using this approach the directivity patterns of the different configurations of the transducer arrays consisting of eight elements have been calculated. The velocities of  $A_0$  and  $S_0$  modes of Lamb waves used in calculations are presented in Table 2. These parameters correspond to the Lamb wave velocities in 10mm thickness aluminium plate at the 70kHz frequency.

The directivity patterns were calculated at the distance 5m using the 5 periods burst with the Gaussian envelope. The waveform of the signal is presented in Fig.8.

Table 2. The Lamb wave velocities used in the calculations

Velocity	$A_0$ , m/s	$S_0$ , m/s
Phase	2110	5397
Group	3065	5310

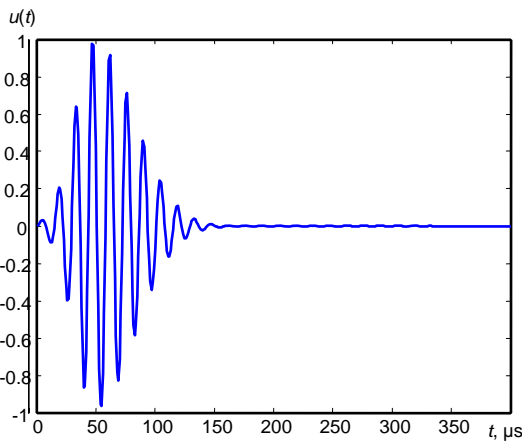


Fig.8. The waveform of the signal used in the directivity pattern calculations

It was assumed that a single transducer generates both  $A_0$  and  $S_0$  modes of the Lamb waves propagating in all direction. Such an assumption is close to reality when the pressure or longitudinal type transducer is used. The obtained directivity patterns of the different types of transducers arrays are presented in Fig.9-15. In the right upper corner of the figures the type of the transducer is denoted. By the solid line is shown the directivity pattern of the  $A_0$  mode, by the dashed line – of the  $S_0$  mode. As can be seen in most cases both  $A_0$  and  $S_0$  modes of the Lamb waves are generated. The big side lobes at least of one of the modes can be observed almost in all cases. From

the presented figures follows that most promising for  $A_0$  generation is a horizontal array with a spacing  $\lambda_{A0}/2$  (Fig.10) and the matrix transducer array 2x4 (Fig.15) with the horizontal spacing  $\lambda_{A0}/2$  and the vertical spacing  $\lambda_{A0}$ . The selection of the most optimal transducer array is based on the following criteria – the biggest front lobe of the directivity pattern and the smallest side lobes, because side lobes create multiple reflections across the plate. In the case of the horizontal array (Fig.10) the strong generation of  $S_0$  occurs also, but side lobes are slightly smaller comparing to the transducer array 2x4.

More complicated results are obtained when the distance between transducers corresponds to the wavelength or half wavelength of the symmetric Lamb wave mode  $S_0$  (Fig.16-22). The regularities of the directivity patterns of the  $S_0$  mode are similar to those which were obtained for  $A_0$  (Fig.10-15) with a corresponding distance between transducers. However the directivity patterns of the  $A_0$  mode are much more complicated. In all cases (Fig.16-22) the multiple side lobes can be observed. So, it can be stated that in any case of the analyzed transducer arrays except the desired  $S_0$  mode always undesired  $A_0$  mode waves with a relatively strong amplitude will be generated.

The directivity patterns of a few more types of the transducer arrays are presented in Fig.23-24. One of them is more efficient for excitation of the  $S_0$ , another one of  $A_0$  modes and both has relatively low level lobes of the  $A_0$  mode. The last one is 2x4 inverted array, that is, the transducer of the second row are excited using the signals of an opposite polarity. Such a transducer array have one lobe of  $S_0$  mode, but several side lobes of  $A_0$  mode generated approximately at 45° angle to the main direction.

Comparing the amplitudes of the  $S_0$  and the  $A_0$  modes in the directivity pattern it is necessary to take into account that a true ratio of their amplitudes very depends on the excitation efficiency, which should be determined by a numerical modelling and/or experimentally and was not taken into account in the presented results.

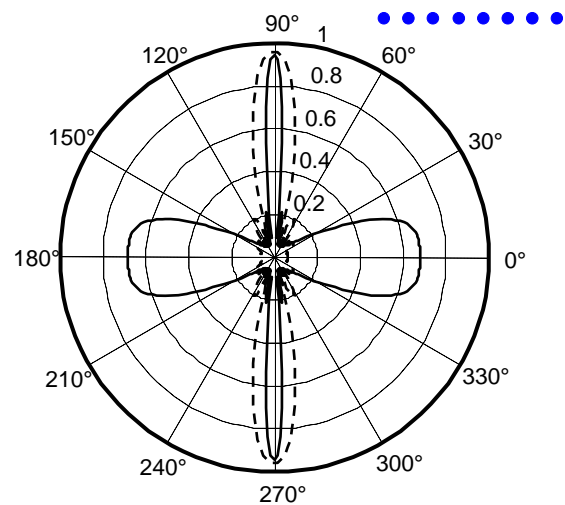


Fig.9. The directivity pattern of the “horizontal” 8 element longitudinal (excitation normal to the surface) transducer array. The spacing is  $\lambda_{A0}$ : solid line –  $A_0$  mode dashed line –  $S_0$  mode

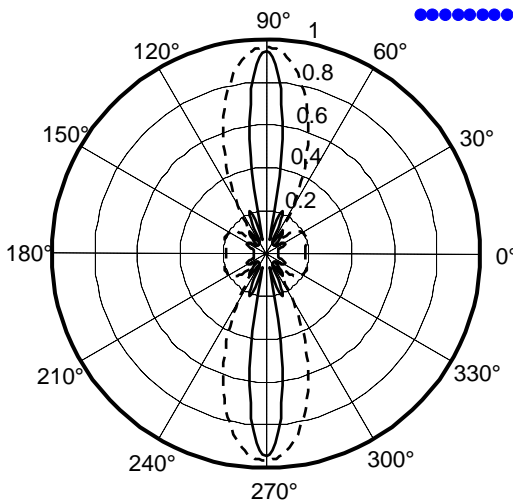


Fig.10. The directivity pattern of the “horizontal” 8 element transducer array. The spacing is  $\lambda_{A0}/2$ : solid line –  $A_0$ , dashed line –  $S_0$

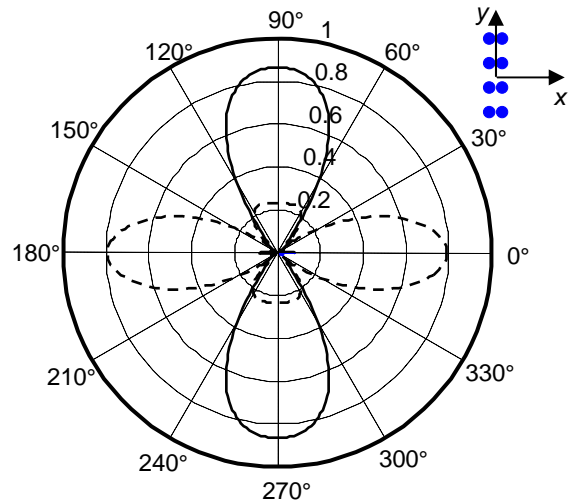


Fig.13. The directivity pattern of the transducer array 4x2. The spacing along axis  $x$  is  $\lambda_{A0}/2$ , along  $y$  axis is  $\lambda_{A0}$ : solid line –  $A_0$ , dashed line –  $S_0$

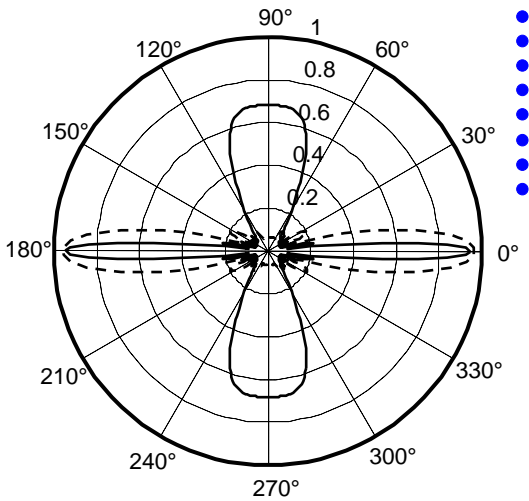


Fig.11. The directivity pattern of the “vertical” 8 element transducer array. The spacing is  $\lambda_{A0}$ : solid line –  $A_0$ , dashed line –  $S_0$

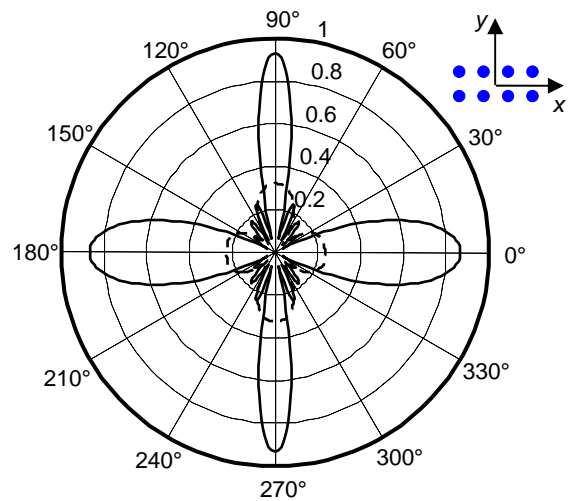


Fig.14. The directivity pattern of the transducer array 2x4. The spacing along both axes is equal to wavelength of  $A_0$  mode  $\lambda_{A0}$  solid line –  $A_0$ , dashed line –  $S_0$

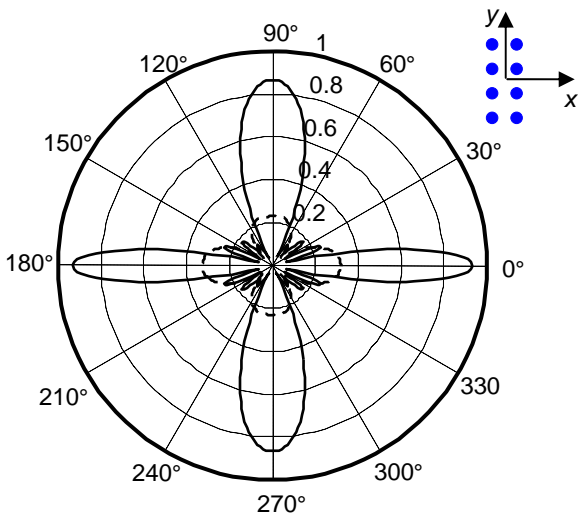


Fig.12. The directivity pattern of the transducer array 4x2. The spacing along both axes is equal to wavelength of  $A_0$  mode  $\lambda_{A0}$ : solid line –  $A_0$ , dashed line –  $S_0$

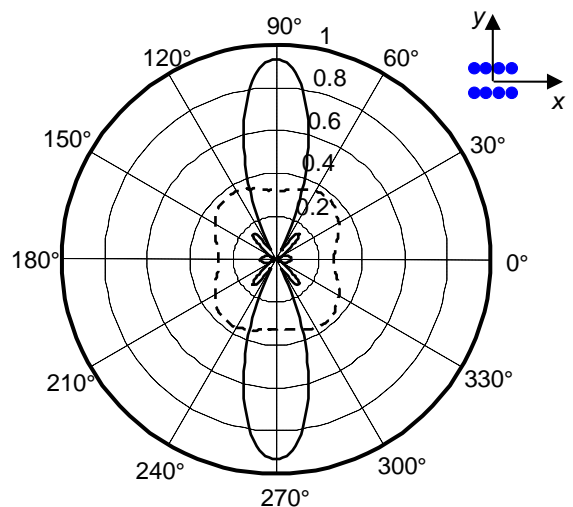


Fig.15. The directivity pattern of the transducer array 2x4. The spacing along axis  $x$  is  $\lambda_{A0}/2$ , along  $y$  axis is  $\lambda_{A0}$ : solid line –  $A_0$ , dashed line –  $S_0$



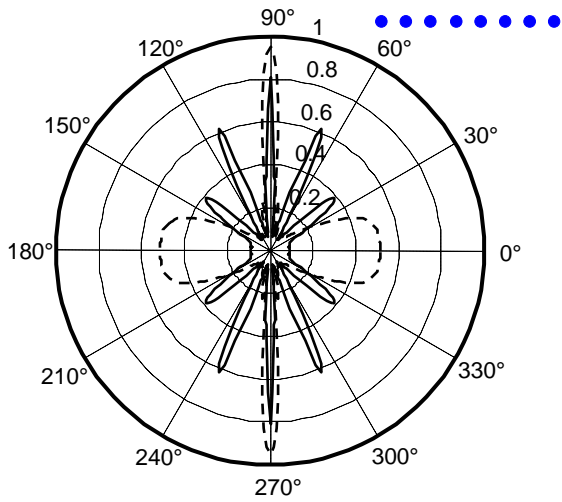


Fig.16. The directivity pattern of the “horizontal” 8 element transducer array. The spacing is  $\lambda_{s0}$ : solid line –  $A_0$ , dashed line –  $S_0$

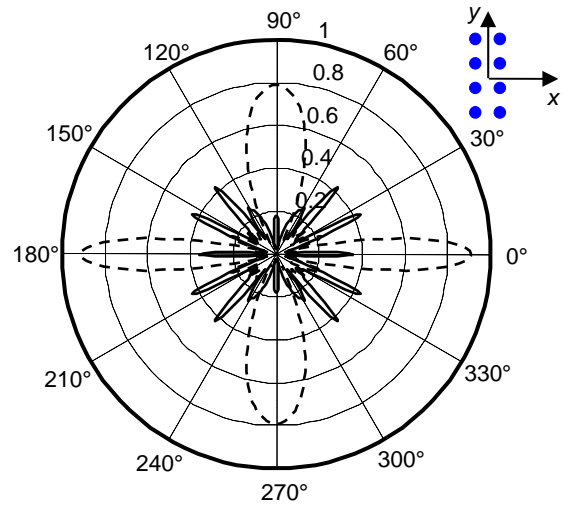


Fig.19. The directivity pattern of the transducer array 4x2. The spacing along both axes is equal to wavelength of  $A_0$  mode  $\lambda_{s0}$ : solid line –  $A_0$ , dashed line –  $S_0$

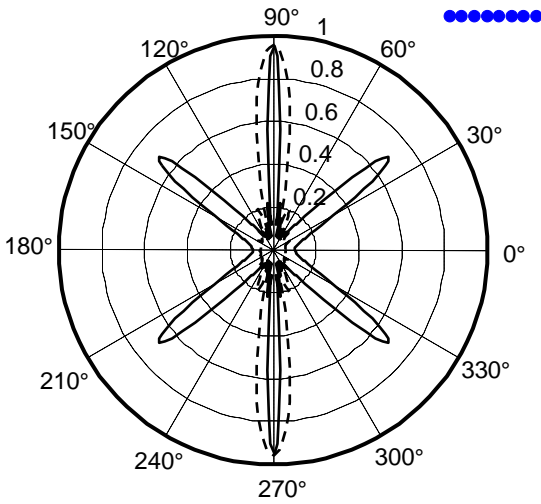


Fig.17. The directivity pattern of the “horizontal” 8 element transducer array. The spacing is  $\lambda_{s0}/2$ : solid line –  $A_0$ , dashed line –  $S_0$

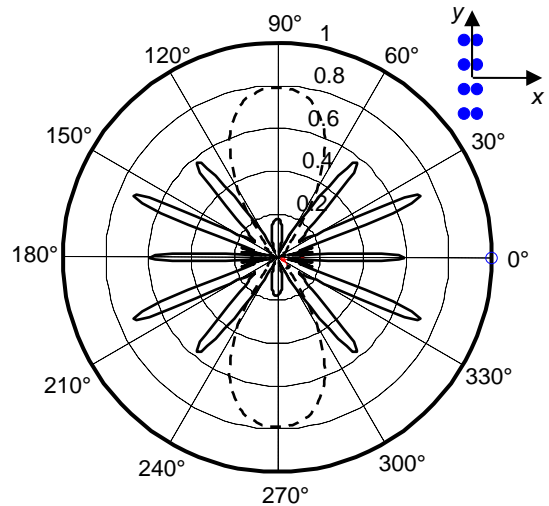


Fig.20. The directivity pattern of the transducer array 4x2. The spacing along axis  $x$  is  $\lambda_{x0}/2$ , along  $y$  axis is  $\lambda_{s0}$ : solid line –  $A_0$ , dashed line –  $S_0$

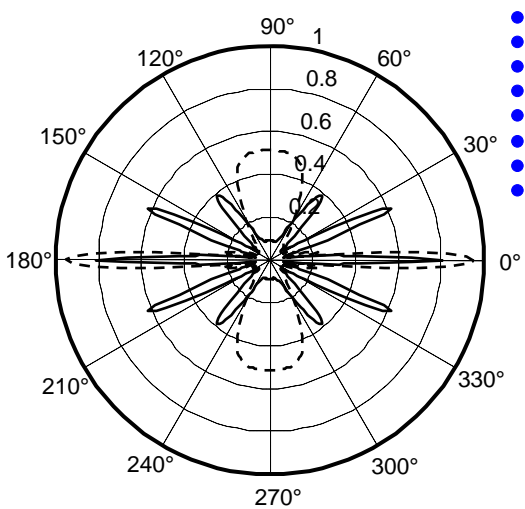


Fig.18. The directivity pattern of the “vertical” 8 element transducer array. The spacing is  $\lambda_{s0}$ : solid line –  $A_0$ , dashed line –  $S_0$

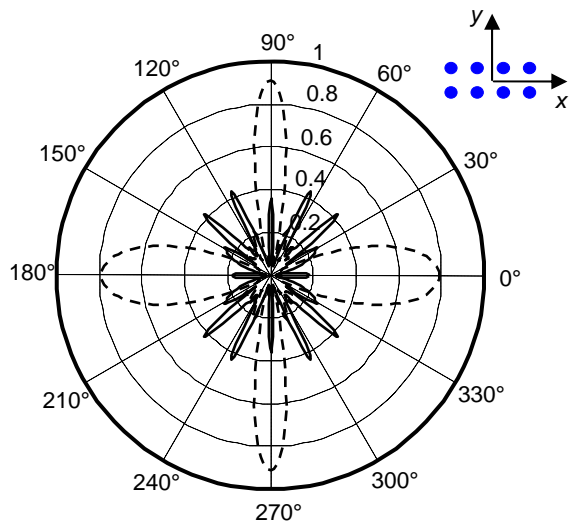


Fig.21. The directivity pattern of the transducer array 2x4. The spacing along axis is equal to wavelength of  $A_0$  mode  $\lambda_{s0}$ : solid line –  $A_0$ , dashed line –  $S_0$

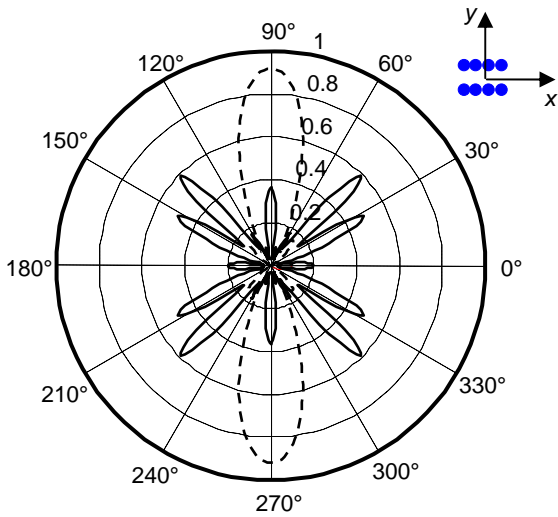


Fig.22. The directivity pattern of the transducer array 2x4. The spacing along axis  $x$  is  $\lambda_{s0}/2$ , along  $y$  axis is  $\lambda_{s0}$ : solid line –  $A_0$ , dashed line –  $S_0$

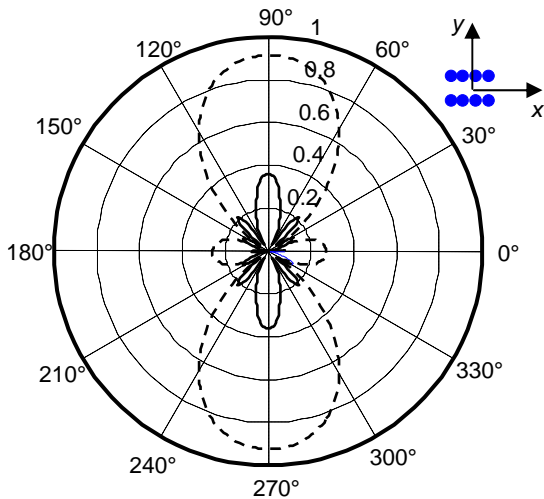


Fig.23. The directivity pattern of the transducer array 2x4. The spacing along axis  $x$  is  $\lambda_{\lambda 0}/2$ , along  $y$  axis is  $\lambda_{s0}$ : solid line –  $A_0$ , dashed line –  $S_0$

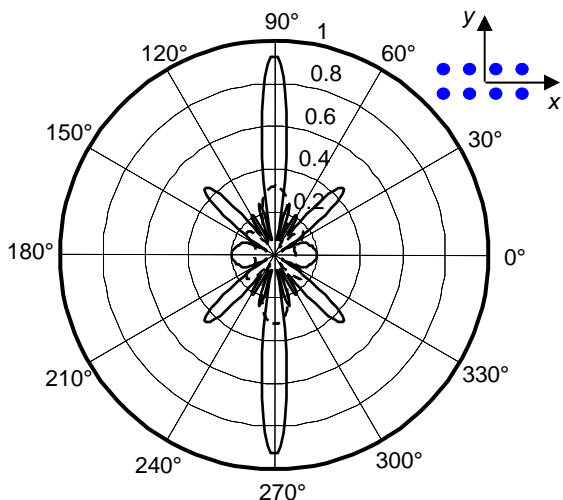


Fig.24. The directivity pattern of the transducer array 2x4. The spacing along axis  $x$  is  $\lambda_{s0}/2$ , along  $y$  axis is  $\lambda_{\lambda 0}$ : solid line –  $A_0$ , dashed line –  $S_0$

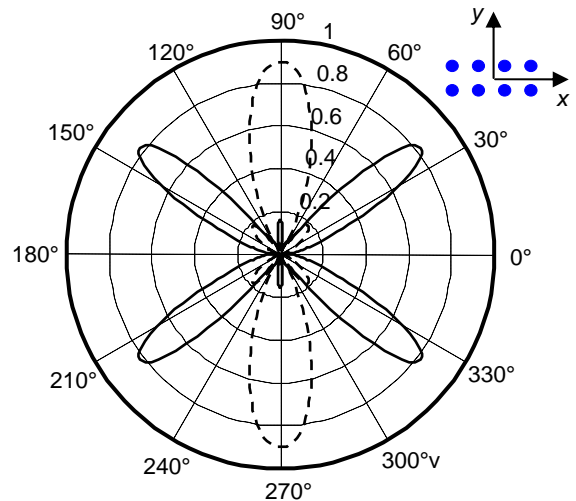


Fig.25. The directivity pattern of the inverted 2x4 transducer array. The spacing along axis  $x$  is  $\lambda_{s0}/2$ , along  $y$  axis is  $\lambda_{\lambda 0}$ : solid line –  $A_0$ , dashed line –  $S_0$

### Directivity patterns of array in the case of the shear type transducers

The directivity patterns of the arrays exploiting shear type transducers were calculated taking into account directivity patterns of a single element which were obtained using the finite element modelling. So, the integral signals of  $A_0$  and  $S_0$  modes at the observation point were calculated according to

$$u_{\Sigma, A_0}(\alpha, t) = \sum_{k=1}^{N_{te}} d_{A_0}(a) \cdot u_k(\alpha, t), \quad (7)$$

$$u_{\Sigma, S_0}(\alpha, t) = \sum_{k=1}^{N_{te}} d_{S_0}(a) \cdot u_k(\alpha, t). \quad (8)$$

The obtained directivity patterns for several configurations of transducer arrays are presented in Fig. 26-28. In general, the similar regularities can be observed, except that side lobes are essentially reduced. The side lobes perpendicular to the main direction almost completely disappeared.

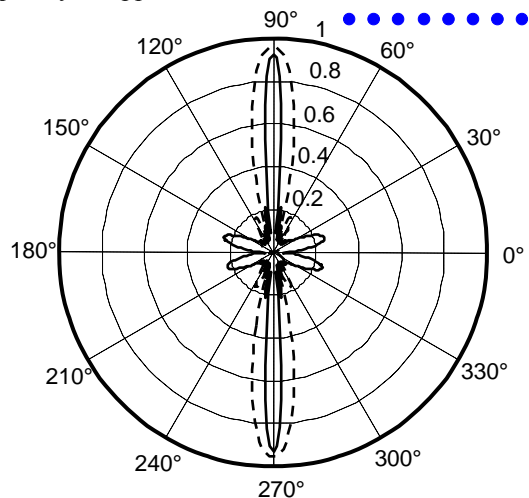


Fig.26. The directivity pattern of the "horizontal" 8 element shear type transducer array. The spacing is  $\lambda_{\lambda 0}$ : solid line –  $A_0$ , dashed line –  $S_0$

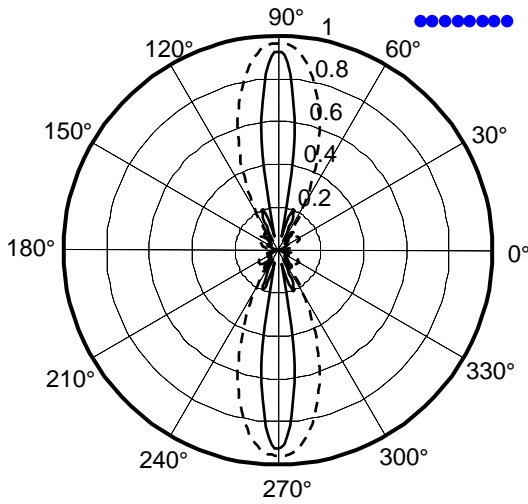


Fig.27. The directivity pattern of the “horizontal” 8 element shear type transducer array. The spacing is  $\lambda_{A0}/2$ : solid line –  $A_0$ , dashed line –  $S_0$

time technique is the possibility to reduce of the amplitude of the backward lobe. The second advantage is that the dimensions of the transducer array are not critical.

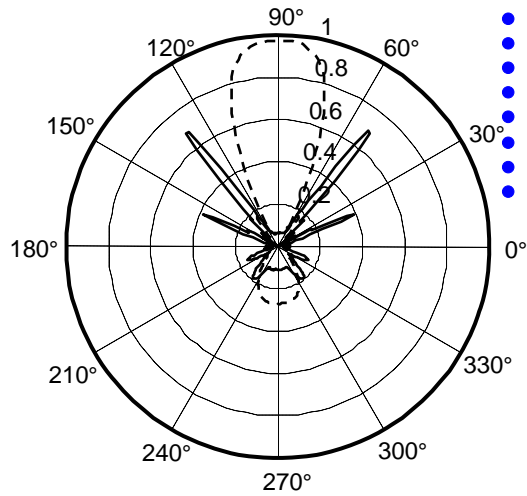


Fig.29. The directivity pattern of the “vertical” 8 element shear type transducer array. The spacing is  $\lambda_{S0}$ : solid line –  $A_0$ , dashed line –  $S_0$

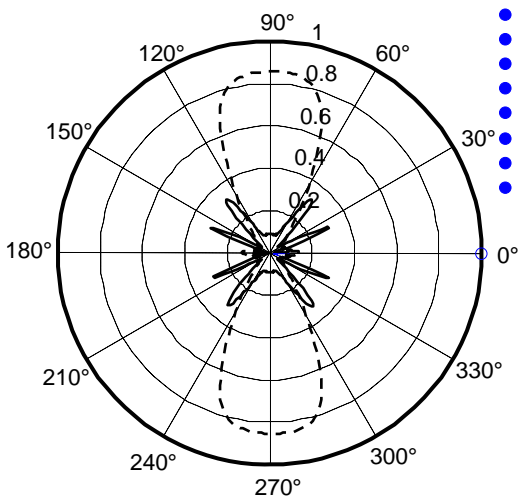


Fig.28. The directivity pattern of the “vertical” 8 element shear type transducer array. The spacing is  $\lambda_{S0}$  solid line –  $A_0$ , dashed line –  $S_0$

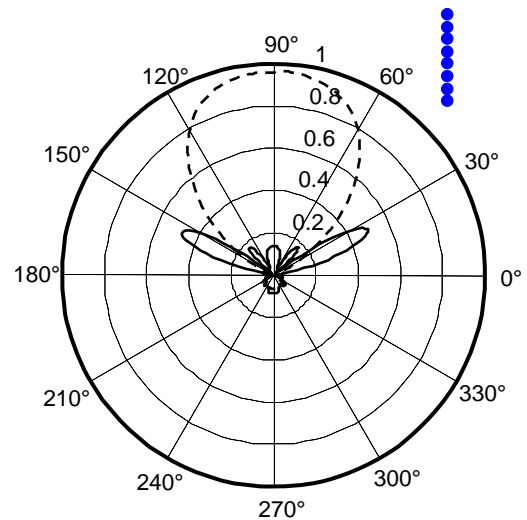


Fig.30. The directivity pattern of the “vertical” 8 element shear type transducer array. The spacing is  $\lambda_{A0}/2$  solid line –  $A_0$ , dashed line –  $S_0$

### Comparison of simultaneous excitation of transducer array and excitation using time delay

In the experiments and calculations presented above it was assumed that all elements of the transducer array were excited at the same instance. The control of the directivity and the efficiency of the transducer array were implemented by changing the distances between the elements. On the other hand, the control of the transducer array can be performed by introducing individual delay times for each element. The objective of this stage of investigation was to determine what difference in the performance of transducer arrays can be expected when one or another excitation technique is used. With the purpose to clarify this question the directivity patterns of a “vertical” transducer array with different spacing were calculated in the case when the delay time technique is used. The obtained results are presented in Fig.29-30. The results demonstrate that the main advantage of the delay

### Conclusion

The main conclusions of the research carried out are the following:

1. There are two factors that complicate interpretation of the waveforms of received signals: almost in all cases of the arrays both  $A_0$  and  $S_0$  modes of Lamb waves and also Lamb waves in lateral directions are generated.
2. The “horizontal” transducer arrays in all cases generate both  $A_0$  and  $S_0$  modes of Lamb waves. Selective generation of only  $A_0$  or  $S_0$  mode waves can be implemented only by application of “vertical” or matrix transducer arrays.



3. In the case of the longitudinal type of transducers the smallest side lobes in the directivity patterns possess the following arrays:
  - the “horizontal” array with the spacing  $\lambda_{A_0}/2$  generating  $A_0$  and  $S_0$  mode waves;
  - the array 2x4 having spacing  $\lambda_{A_0}/2$  in the “horizontal” direction and  $\lambda_{A_0}$  in the “vertical” direction generating mainly  $A_0$  mode wave;
  - the array 2x4 having spacing  $\lambda_{A_0}/2$  in the “horizontal” direction and  $\lambda_{S_0}$  in the “vertical” direction generating mainly  $S_0$  mode waves;
4. The arrays with the shear type transducers possess essentially smaller side lobes, comparing with the arrays based on longitudinal type of the transducers, especially in the lateral direction.
5. Due to the simultaneous excitation technique the directivity patterns of all types of transducer arrays are symmetric with respect to both axis (horizontal and vertical). As a consequence, the waves in front and back directions are generated of the same amplitude. The waves generated in the backward direction are reflected by the edge of the plate and complicate interpretation of the results.
6. The application of the delay time excitation technique enables essentially to reduce the amplitude of the signal generated in the backward direction.

### Acknowledgements

The part of this work was sponsored by the European Union under the Framework-6 LRUCM project. The

Project is coordinated and managed by TWI (UK). Ref.: Coll-CT-2005-516405.

### References

1. **Mudge P. J.** Field Application of the Teletest<sup>®</sup> Long-Range Ultrasonic Testing Technique, Insight. 2001. Vol.43. P.74- 77.
2. **Song.W.-J., Rose J. J., Whitesel H.** An ultrasonic guided waves technique for damage testing in a ship hull. Materials Evaluation. 2003. Vol.60. P. 94-98.
3. **Cawley P., Lowe M. J. S., Alleyne D. N, Pavlakovic B. and Wilcox P.** Practical long range guided wave testing: Applications to Pipes and Rail, Mat. Evaluation. 2003. Vol.61. P. 66-74.
4. **Kwun H., Kim S. Y. and Light G. M.** The magnetostrictive sensor technology for long-range guided- wave testing and monitoring of structures. Evaluation. 2003. Vol.61. P. 80-84.

L. Mazeika, R. Kažys, A. Maciulevičius

### Ultragarsinių gardelių Lembo bangoms žadinti optimizavimas

#### Reziumė

Nukreiptosios bangos naudojamos didelėms pramoninėms konstrukcijoms tikrinti. Plokščiuose objektuose sklindančios Lembo bangos tiktų defektams aptikti metalo plokštėse ar jų gaminiuose. Tokioms bangoms žadinti naudojamos ultragarsinės gardelės. Šio darbo tikslas buvo ištirti įvairios konfigūracijos Lembo bangų žadinimo gardelių kryptines savybes. Baigtinių elementų metodu buvo nustatytos vieno gardelės elemento kryptingumo diagramos išilginių ir skersinių bangų keitiklių atvejais. Naudojant gautąsias kryptines elementų charakteristikas buvo apskaičiuotos įvairios konfigūracijos aštuonių elementų gardelių kryptingumo diagramos. Jos parodė, kad daugeliu atvejų žadinamos tiek simetrinė  $S_0$ , tiek asimetrinė  $A_0$  Lembo bangų modos. Be to, gana ryškūs yra šoniniai lapeliai. Kaip tyrimų rezultatas buvo nustatytos optimalios gardelių konfigūracijos, įgalinančios žadinti norimą Lembo bangų modą esant minimaliam šoninių lapelių ir parazitinių modų lygiui.

Pateikta spaudai 2007 12 12